ELSEVIER

LETTER TO THE EDITOR

Establishment of suction blister roof grafting by injection of local anesthesia beneath the epidermis: Less painful and more rapid formation of blisters

The number of patients suffering from diabetic foot ulcers [1] and rheumatic ulcers [2] is increasing rapidly. Vitiligo is an acquired depigmented skin disorder that results from the destruction of melanocytes with unknown etiology. Suction blisters were first used for the transplantation of viable epidermis in vitiligo lesions and chronic wounds [3], followed by a simplified modification to form blisters [4]. We have previously reported the usefulness of epidermal sheet grafts to treat intractable skin ulcers caused by autoimmune diseases [2], diabetes mellitus [1] or other diseases [5,6] through their unique actions that differ from conventional skin grafts that include dermal components [7,8].

The technique to use syringes and three-way stopcocks to form suction blisters is comparatively simple and conservative, but it has two major problems. One is the time required to make blisters; Gupta and Kumar reported that as long as 78, 98 and 123 min are required to generate suction blisters when 5, 10 and 20 ml syringes are used, respectively [9], which is one reason why this simple technique is not used more commonly to treat chronic wounds. The other problem is the pain caused by the procedure; negative pressure at donor sites sometimes causes pain, which imposes a great burden on the patient.

The original method [3] and its modifications [4,9] do not use local anesthesia except for a case report [10], which did not emphasize the impor-

tance of the injection depth, and consequently time required to generate suction blister (T-SB) they measured varied from 30 min to as long as 3 h [10]. There have been no reports comparing methods with or without local anesthesia in terms of pain relief and T-SB.

All procedures were performed in accordance with the ethical standards of the Helsinki Declaration of 1975. Sixty-nine sites from 61 patients were enrolled in this retrospective study (Table 1). Thirty-nine sites in 34 patients did not receive anesthesia, whereas 30 sites in 27 patients received anesthesia. We injected 1.0–1.5 ml/cm^2 of 0.5–1.0% lidocaine without epinephrine as a local infiltration anesthetic just beneath the epidermis. Two meticulous techniques are required. First, it is important to confirm the resistance produced by spreading the dense dermal tissue with the liquid. The resistance is less when the injection is made into the sub-reticular dermis or into the subcutaneous fatty layer by mistake. Second, it must be emphasized that the insertion sites for the needle should not be used as donor areas since that hampers the subsequent formation of blisters.

We first investigated the pain relief between the two groups using the chi-square test (JMP6 software, SAS, Cary, NC, USA). As expected, the pain caused by the negative pressure was eliminated in cases where anesthesia was used ($n = 27$), whereas 11 out of 22 patients without anesthesia felt pain ($p = 0.001$).

We then measured T-SB to investigate whether that was reduced when anesthetics were injected into the sub-epidermis before producing the suction blister (Fig. 1A). The average T-SB without anesthesia was 65.0 $\pm$ 6.7 (average $\pm$ standard error), 98.3 $\pm$ 5.0 or 128.6 $\pm$ 11.6 min for syringes with capacities of 5 ml ($n = 8$), 10 ml ($n = 24$) or 20 ml ($n = 7$), respectively, consistent with the previous report [9]. When local anesthesia was used at the donor site, the T-SB with 5 ml ($n = 4$), 10 ml ($n = 21$) or 20 ml ($n = 6$) syringes was 16.7 $\pm$ 4.1, 23.6 $\pm$ 1.5 or 42.5 $\pm$ 4.2 min, respectively. The T-SB was significantly decreased as short as one-fourth of the

Table 1 Summary of the patients who received local anesthesia to harvest epidermis

Patient number	Age (years)	Sex (F/M)	Basic disease	Syringe (ml)	T-SB (min)	T-SB/cm² (min)	Wound site	Wound size (cm²)	Major infection	Bone exposure or osteomyelitis	Amputation	Healing period (weeks)
1	67	F	SSc	10	20	9.95	Toes, foot, fingers	40	MRSA	+	+ (Major)	N/A
2	77	F	PAN	20	40	12.74	Leg	10	MRSA			6
2'	77	F	PAN	20	40	12.74	Leg	1	MRSA			6
3	75	F	DM	5	10	6.49	Toe	2.5	Serratia marcescens	+		4
4	78	M	ASO, CRF	10	40	19.90	Toe	3	MRSA, Ps. aeruginosa	+		12
5	69	M	DM	20	35	11.15	Foot	3	MRSA	+		10
6	73	F	SJS	5	20	12.99	Foot	12	MRSA	+		10
7	71	M	MM	20	60	19.11	Foot	5	Negative			6
7'	71	M	MM	10	25	12.44	Foot	25	Negative			6
8	59	F	CREST	10	20	9.95	Toes, foot	15	MRSA	+		12
9	76	M	DM, CCE	10	20	9.95	Toes, foot	10	MRSA	+		15
9'	76	M	DM, CCE	20	45	14.33	Toes, Foot	10	MRSA	+		15
10	44	F	SLE	10	25	12.44	Finger	7.5	Negative	+		7
11	48	M	PAN	20	35	11.15	Leg, toe, foot	100	Negative	+	+	N/A
12	48	M	PAN	10	25	12.44	Leg, toe, foot	100	Negative	+	+	N/A
13	91	M	DM	10	30	14.93	Toes	2.5	MRSA, Ps. aeruginosa	+		7
14	85	M	DM	5	20	12.99	Toes	0.4	MRSA, Ps. aeruginosa			4
15	70	F	SSc	5	15	9.95	Finger	150	MRSA			5
16	70	M	VU	10	20	9.95	Leg	45	Negative			15
17	45	F	VU	10	25	12.44	Leg	50	MRSA			3
18	35	M	VU	10	30	14.93	Leg	4	Serratia marcescens			6
19	76	M	VU	10	25	12.44	Leg	20	MSSA			
20	81	F	APS	10	15	7.46	Leg	50	Negative			
21	58	F	MRA	10	15	7.46	Leg	30	MSSA			
22	55	F	VU	10	20	9.95	Leg	2	MSSA			
23	61	F	SSc	10	20	9.95	Foot	5	MRSA	+		
24	31	F	SLE	10	30	14.93	Leg, Abd, back	70	MRSA			
25	58	F	SLE	10	35	17.41	Foot, fingers	20	MRSA			
26	70	M	DM	10	20	9.95	Toes	30	MRSA			
27	73	M	DM	10	20	9.95	Toes	10	MRSA	+		
Average	65.6	F:M=15:15				12.1		27.8		(+: =13:17)	(+: =3:27)	8.3
S.E.	2.9					0.6		7.1				0.9

SSc, systemic sclerosis; PAN, polyarteritis nodosa; DM, diabetes melitus; ASO, arteriosclerosis obliterans; CRF, chronic renal failure; SjS, Sjogren's syndrome; MM, malignant melanoma; CCE, cholesterol crystal embolism; SLE, systemic lupus erythematosus; VU, venous ulcer; APS, anti-phospholipid syndrome; MRA, malignant rheumatoid arthritis; MRSA, methicillin-resistant Staphylococcus aureus; Ps. aeruginosa, Pseudomonas aeruginosa; T-SB, time required to generate suction blister. Major amputation means amputation below the knee. This table summarizes personal patient data in the group with anesthesia, focusing on the pathogenic cause of skin ulcers, wound sites and wound sizes. From February 1st 2006 to October 31st 2007, 27 Asian patients with finger, leg or foot ulcers received local anesthesia to obtain blisters at the Osaka University Medical Hospital and at the Nagoya City University Hospital, Nagoya, Japan. Patients 2 and 7 received secondary epidermal grafts because of their multiple wound lesions. The reason why the T-SB was 40 min with the 10 ml syringe in Patient 4 is probably because the negative pressure was comparatively weaker due to leakage during the procedure. It took 60 min with a 20 ml syringe in Patient 7 probably because the anesthetic had been injected into the sub-reticular dermis, not into the sub-epidermis, due to an error by the operator. We used both 10 and 20 ml syringes at the same time in Patient 9. Personal patient data in the group without anesthesia are obtained from December 17th 1998 to February 14th 2002, and are published elsewhere [1,2,5,6].
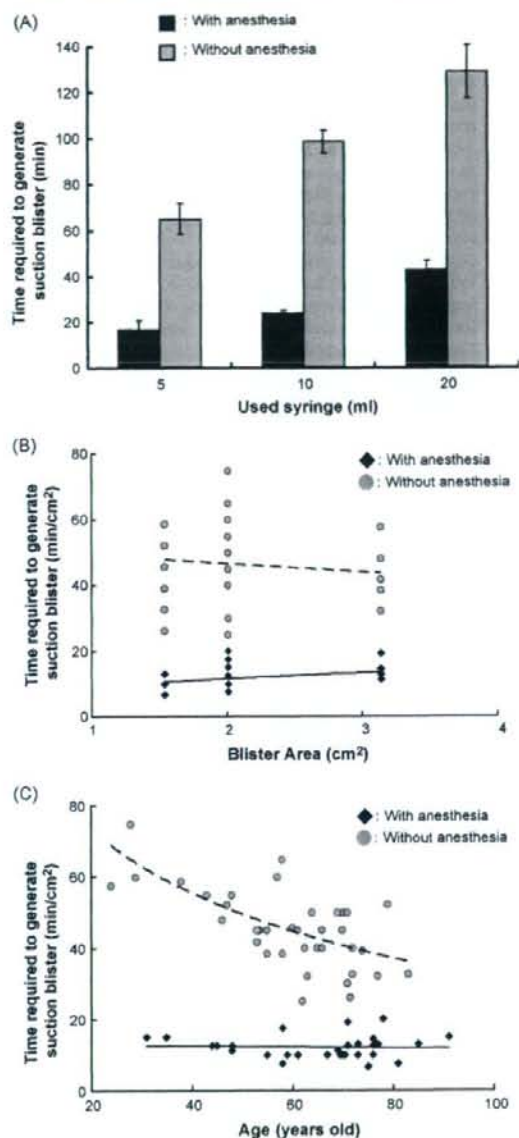
time originally reported in all syringe sizes used in the group with anesthesia: 5 ml ($p = 0.00008$), 10 ml, ($p < 0.00001$) and 20 ml ($p = 0.0001$) as determined by Student's t-test. We neither experienced any failure in producing suction blisters with this procedure nor any adverse side effects, including allergy against the anesthetic.

We compared the healing periods between groups with ($n = 18$; 8.3 0.9 weeks; Table 1) or without anesthesia. After the wound bed had been prepared for the grafting, the epidermis obtained by either method was accepted well and healed similarly. We have confirmed the efficacy of epidermal grafting as previously reported in addition to the usefulness of bone marrow exposure, which promotes wound healing by enhancing granulation tissue formation. Exclusion criteria for the use of epidermal grafting would be severe infection and calcific uremic arteriolopathy (calciphylaxis).

We finally investigated whether the T-SB is shorter in older patients than in younger patients. For this purpose, we compared the T-SB divided by the area among the three different sized syringes used (Fig. 1B). The areas of epidermal sheets produced by 5, 10 and 20 ml syringes were 1.54, 2.01 and 3.14 cm^2, respectively. The T-SB/cm^2 was similar regardless of the size of syringe both in groups with anesthesia ($p = 0.329$; $r^2 = 0.087$) or without anesthesia ($p = 0.491$; $r^2 = 0.013$), suggesting that the parameter of T-SB/cm^2 can be used instead of the T-SB in each syringe size to investigate the correlation with age. This finding also suggested that it is better to apply multiple smaller syringes to obtain epidermis in a shorter period of time although large sheets of epidermis to cover large areas of wounds cannot be obtained that way.

The T-SB/cm^2 did not correlate with patient age in the group with anesthesia ($n = 30$; $p = 0.342$; $r^2 = 0.003$), whereas it correlated inversely with age in the group without anesthesia ($n = 39$; $p < 0.0001$; $r^2 = 0.481$). This suggests that the T-SB is shorter in

Fig. 1 Rapid formation of suction blister roof by injection of local anesthesia beneath the epidermis. (A) The comparison of time required to generate suction blister (T-SB) with (black bars) or without (gray bars) anesthesia using 5, 10 or 20 ml syringes. When measuring the T-SB (and the pain relief), the lower abdomen or the anterior thigh is used as the donor site to avoid anatomical differences in the T-SB and in the sensory nervous system. JMP6 software is used for statistical analyses using Student's t-test. Values are expressed as averages standard error. When the sub-epidermal anesthetic is used, the T-SB is significantly decreased in all syringe sizes: 5 ml ($p = 0.00008$), 10 ml, ($p < 0.00001$) and 20 ml ($p = 0.0001$). (B) The comparison of T-SB/cm^2 in groups with (black rhomboid dots) or without (gray circle dots) anesthesia. The T-SB/cm^2 is similar regardless of the size of syringe both in groups with anesthesia ($p = 0.329$; $r^2 = 0.087$) or without anesthesia ($p = 0.491$; $r^2 = 0.013$). (C) The comparison of patient age and T-SB with (black rhomboid dots) or without (gray circle dots) anesthesia. Since elderly people have loose skin tissue with a paper-like appearance, it might be easier to form suction blisters in older patients. Our results show that the T-SB correlates negatively with the age of patients when anesthesia is not used ($n = 39$; $p < 0.0001$; $r^2 = 0.481$), but does not correlate with age when anesthesia is used ($n = 30$; $p = 0.342$; $r^2 = 0.003$).

older patients only when anesthesia is not used and that the sub-epidermal anesthetic dramatically accelerates the T-SB in younger patients (Fig. 1C).

Since the time required for the anesthesia to take effect should be less than 5 min, the total time to form blisters is still much shorter when the local anesthesia is used. This method becomes applicable to patients at high risk of pressure sores. Economically speaking, the cost performance is significantly improved by shortening the time required for the procedure; this epidermal grafting by itself costs approximately $500 for an area of less than 25 cm^2 in Japan. We now established how to harvest suction blister roofs simply by injection of local anesthesia beneath the epidermis, resulting in a less painful and more rapid way to form blisters.

Funding sources

Statement on prior presentation

None reported.

References

[1] Yamaguchi Y, Yoshida S, Sumikawa Y, Kubo T, Hosokawa K, Ozawa K, et al. Rapid healing of intractable diabetic foot ulcers with exposed bones following a novel therapy of exposing bone marrow cells and then grafting epidermal sheets. Br J Dermatol 2004;151:1019–28.

[2] Yamaguchi Y, Sumikawa Y, Yoshida S, Kubo T, Yoshikawa K, Itami S. Prevention of amputation caused by rheumatic diseases following a novel therapy of exposing bone marrow, occlusive dressing and subsequent epidermal grafting. Br J Dermatol 2005;152:664–72.

[3] Falabella R. Epidermal grafting. An original technique and its application in achromic and granulating areas. Arch Dermatol 1971;104:592–600.

[4] Mukhtar M, Singh S, Shukla VK, Pandey SS. Surgical pearl: suction syringe for epidermal grafting. J Am Acad Dermatol 1997;37:638–9.

[5] Yamaguchi Y, Kubo T, Tarutani M, Sano S, Asada H, Kakibuchi M, et al. Epithelial–mesenchymal interactions in wounds: treatment of palmoplantar wounds by nonpalmoplantar pure epidermal sheet grafts. Arch Dermatol 2001;137:621–8.

[6] Yamaguchi Y, Yoshikawa K. Cutaneous wound healing: an update. J Dermatol 2001;28:521–34.

[7] Yamaguchi Y, Itami S, Watabe H, Yasumoto K, Abdel-Malek ZA, Kubo T, et al. Mesenchymal—epithelial interactions in the skin: increased expression of dickkopf1 by palmoplantar fibroblasts inhibits melanocyte growth and differentiation. J Cell Biol 2004;165:275–85.

[8] Yamaguchi Y, Passeron T, Hoashi T, Watabe H, Rouzaud F, Yasumoto K, et al. Dickkopf 1 (DKK1) regulates skin pigmentation and thickness by affecting Wnt/β-catenin signaling in keratinocytes. Faseb J 2007.

[9] Gupta S, Kumar B. Suction blister induction time: 15 min or 150 min? Dermatol Surg 2000;26:754–6.

[10] Suga Y, Butt KI, Takimoto R, Fujioka N, Yamada H, Ogawa H. Successful treatment of vitiligo with PUVA-pigmented autologous epidermal grafting. Int J Dermatol 1996;35:518–22.

Takaaki Hanafusa[1]
Department of Dermatology, Osaka University Graduate School of Medicine, Japan

Yuji Yamaguchi[,1,*]
Department of Dermatology, Osaka University Graduate School of Medicine, Japan

Department of Geriatric and Environmental Dermatology, Nagoya City University Graduate School of Medical Sciences, Japan

Motoki Nakamura[1]
Reiko Kojima
Rieko Shima
Yoshiko Furui
Shoichi Watanabe
Aiko Takeuchi
Natsumi Kaneko
Yoichi Shintani
Akira Maeda
Department of Geriatric and Environmental Dermatology, Nagoya City University Graduate School of Medical Sciences, Japan

Mamori Tani
Department of Dermatology, Osaka University Graduate School of Medicine, Japan

Akimichi Morita
Department of Geriatric and Environmental Dermatology, Nagoya City University Graduate School of Medical Sciences, Japan

Ichiro Katayama
Department of Dermatology, Osaka University Graduate School of Medicine, Japan

*Corresponding author at:
Department of Geriatric and Environmental
Dermatology, Nagoya City University Graduate
School of Medical Sciences, 1-Kawasumi,
Mizuho-cho, Mizuho-ku,
Nagoya 467-8601, Japan.
Tel.: +81 52 853 8261;
fax: +81 52 852 5449

E-mail address: yujin@med.nagoya-cu.ac.jp
(Y. Yamaguchi)

[1]These three authors contributed equally to this
study.

8 January 2008

Ramified microglial cells promote astrogliogenesis and maintenance of neural stem cells through activation of Stat3 function

Pengxiang Zhu,* Ryuji Hata,*,[1] Fang Cao,* Feng Gu,* Yasushi Hanakawa,[†]
Koji Hashimoto,[†] and Masahiro Sakanaka*

*Department of Functional Histology and [†]Department of Dermatology, Ehime University Graduate School of Medicine, Shitsukawa, Toon, Ehime, Japan

ABSTRACT   The differentiation and proliferation of neural stem cells (NSCs) are regulated by a combination of their intrinsic properties (*e.g.*, transcription factors, epigenetic factors, and microRNA regulation) and cell-extrinsic properties from the microenvironment around NSC (*e.g.*, cytokines, growth factors, and cell-cell contact). Recently, there has been a great interest in clarifying the mechanism of the influence of the microenvironment on NSCs, especially cell-cell contact between NSCs and other types of cells nearby. In this study, we investigated whether microglial (Mi) cells influence the fate of NSCs. Coculture study showed that ramified Mi cells promoted astrogliogenesis and maintenance of NSCs through their paracrine effects. This microglia-induced astrogliogenesis was inhibited by AG490 and by overexpression of the dominant-negative form of Stat3 and SOCS3. Promoter assay revealed transactivation of Stat3 function in NSCs by Mi cells. Gene expression study revealed that mRNA of Notch family members (notch1-3) and sox9 in NSCs was significantly upregulated by Mi cells, and this up-regulation was inhibited by AG490. These results demonstrated that ramified Mi cells promoted astrogliogenesis and maintenance of NSCs by activating Stat3 function and *via* notch and sox9 signaling pathways.—Zhu, P., Hata, R., Cao, F., Gu, F., Hanakawa, Y., Hashimoto, K., Sakanaka, M. Ramified microglial cells promote astrogliogenesis and maintenance of neural stem cells through activation of Stat3 function. *FASEB J.* 22, 3866–3877 (2008)

DURING BRAIN DEVELOPMENT, neural stem cells (NSCs) are produced within germinal zones in close contact with the lateral ventricle walls. The self-renewal, proliferation, and differentiation of NSCs are regulated by the combination of their intrinsic properties (*e.g.*, transcription factors, epigenetic factors, and microRNA regulation) and cell-extrinsic properties from the microenvironment around NSCs: the stem cell niche (*e.g.*, cytokines, growth factors and cell-cell contact; ref. 1). It is reasonable to believe that the interactions between

precursor cells and the microenvironment faced by cells influence their differentiation. In accordance with this hypothesis, astrocytes influence the neuronal fate commitment of adult hippocampal NSCs (2), suggesting the importance of cell-cell interactions between glial cells and NSCs. In addition, recent studies (3, 4) have demonstrated that microglial cells play an important role in neurogenesis.

Microglial cells are hematopoietic in origin and have functions similar to those of other tissue macrophages, including phagocytosis, antigen presentation, and production of cytokines, chemokines, eicosanoids, complement components, matrix metalloproteinases, oxidative radicals, and nitric oxide (NO; ref. 5). In the normal brain, microglial cells display a quiescent phenotype. On insult to the brain, microglial cells became highly activated and express the products mentioned above. Activation of microglial cells can result in either neuroprotective or neurotoxic effects, or both. Even in the quiescent form, microglial cells can express and secrete several neurotrophic factors, as well as several cytokines and chemokines (6).

Because microglial cells have been implicated in a variety of mechanisms of neuronal development and function (7), we investigated the effects of ramified microglial cells that secreted neither interleukin (IL) -6 nor NO on the fate of NSCs. Here, we demonstrated that ramified microglial cells promoted astrogliogenesis and maintenance of NSCs through activation of Stat3 function.

MATERIALS AND METHODS

All experiments were approved by the Ethics Committee of Ehime University Graduate School of Medicine and were conducted according to the Guidelines for Animal Experimentation at Ehime University Graduate School of Medicine.

Neurosphere generation and maintenance

NSCs were isolated from E-17 rats (Wistar rats; Charles River Laboratories, Inc., Yokohama, Japan). The meninges of embryonic rat brains were carefully cleared. The striatal tissue was separated from both hemispheres with fine forceps and was mechanically triturated. Cells were seeded in 9-cm dishes (Sumilon MS13900; Sumitoko Bakelite, Tokyo, Japan) in growth medium composed of Dulbecco modified Eagle medium (DMEM; Sigma Chemical, St. Louis, MO, USA) containing 0.2 mg/ml bovine serum albumin (A-7638, Sigma Chemical), 10 mM HEPES, 4.5 mg/ml glucose, 5 µg/ml insulin, 5 nM sodium selenite, 5 µg/ml transferrin, and 40 ng/ml human recombinant epidermal growth factor (Upstate Biotechnology, Lake Placid, NY, USA). Antibiotics and antimycotics (100 U/ml penicillin and 0.25 µg/ml amphotericin B) were also included. NSCs were grown as neurospheres.

Microglial cell culture

The forebrains of newborn Wistar rats were dissected out, and cell suspensions were obtained by passing the tissues through a nylon mesh (160 µm). The suspended cells were seeded in poly-L-lysine (mean M_r 40,750; Sigma Chemical) -coated 80 cm^2 culture flasks (BD Biosciences, San Jose, CA, USA). They were cultured at 37°C in 5% CO_2 and nearly 100% humidity in DMEM supplemented with 10% fetal calf serum. The culture medium was changed every 2 days. Twelve to 14 days later, microglial cells were isolated according to the method of Suzumura *et al.* (8) with modification. In brief, microglial cells were detached from the astrocyte monolayers in the culture flasks by mechanical shaking and reseeded on 10-cm polystyrene dishes (Suspension Culture Dish; Corning, Corning, NY, USA). The cells were incubated for 10 min at 37°C, and then the dishes were washed twice with serum-free DMEM. The cells attached to the dishes were collected with a scraper and suspended in neurosphere-differentiating medium (Neurobasal medium: Invitrogen, Gaithersburg, MD, USA) containing B27 supplement (Invitrogen), all-trans-retinoic acid (1.0×10^{-7} M), 2 mM L-glutamine, and antibiotics (50 U/ml penicillin and 50 µg/ml streptomycin). Some of the microglial cells were seeded onto 9-cm dishes (Sumilon MS13900; Sumitoko Bakelite) at a density of 1.4×10^5/ml or 4.0×10^5/ml and incubated in the same differentiating medium. Twenty-four hours later, the medium was collected, centrifuged for 15 min at 1500 rpm to remove debris, and used as microglia-conditioned medium (MCM).

Coculture of microglial cells with NSCs

Five days after seeding of triturated cells from the striatal tissue, they were dissociated mechanically and reseeded into poly-L-lysine-coated 24-well plates at a density of 5.0×10^5/ well in neurosphere-differentiating medium (Neurobasal medium; Invitrogen) containing B27 supplement (Invitrogen), all-trans-retinoic acid (1.0×10^{-7} M), 2 mM L-glutamine, and antibiotics (50 U/ml penicillin and 50 µg/ml streptomycin). Four hours later, after we confirmed that NSCs had attached to the bottom of the wells, three types of coculture of NSCs with microglial cells were prepared as follows:

Mixed type

Microglial cells (0, 0.7×10^5, or 2.0×10^5/well) were added directly to NSC cultures in a 24-well plate.

Insert type

Microglial cells (0, 0.7×10^5, or 2.0×10^5/well) were seeded into cell culture inserts (0.4 µm pore size, BD Bioscience) that were placed on the top of a 24-well plate containing NSCs.

Conditioned type

Medium in a 24-well plate containing NSCs was changed to MCM (conditioned medium from 24 h microglia cultures based on neurosphere-differentiating medium at a density of 1.4×10^5/ml or 4.0×10^5/ml). The neurosphere-differentiating medium was changed every 2 days, and MCM was changed every day.

Adenoviral vectors

A recombinant adenovirus expressing human SOCS3 was constructed as described previously (9). Human SOCS3 DNA was excised, and the resultant expression units were inserted at the SwaI site of the cosmid vector pAxCAwt (RBD:1678; Bio Resource Center, Riken, Wako, Japan). To make a dominant-negative form of murine Stat3 (Stat3F), the tyrosine residue at 705 of Stat3 was replaced with phenylalanine (Y705F; ref. 10). Stat3F DNA was excised, and the resultant expression units were inserted at the SwaI site of pAxCAwt. To generate recombinant adenoviruses (Ad.SOCS3 and Ad.Stat3F), cosmid DNA was cotransfected with the DNA-terminal protein complex into human kidney 293 cells. A recombinant adenovirus expressing β-galactosidase (Ad.Lz) was provided by Dr. Izumu Saito (University of Tokyo, Tokyo, Japan). Each recombinant virus was propagated in 293 cells and purified by CsCl step-gradient ultracentrifugation. Viral titers were determined using the modified end point cytopathic effect assay (11).

Application of inhibitors or adenoviral vectors

After growth medium was changed to neurosphere-differentiating medium or MCM, inhibitors or adenoviral vectors were applied to NSCs. The inhibitors used were as follows: LY294002 (CAS 154447–36-6; Promega, Madison, WI, USA) at 10 µm/ml, Noggin (R&D Systems, Minneapolis, MN, USA) at 20 ng/ml, PTP inhibitor II (cat. 540205, CAS 2632–13-5; Calbiochem, La Jolla, CA, USA) at 0.1 nm/ml, and AG490 (cat. 658401; Calbiochem) at 1 µm/ml. Our preliminary experiments revealed that inhibitors had no cytotoxic effects on NSCs at the concentrations used in this study, whereas they showed some cytotoxic effects on NSCs at 10× higher concentrations (data not shown). Adenoviral vectors expressing SOCS3, Stat3F, or Lz [multiplicity of infection (MOI) =10] were also applied to NSCs. For quantitative real-time polymerase chain reaction (PCR) and Western blot analysis, cells were collected at 1 or 3 days after the application of inhibitors or adenoviral vectors.

Immunoblot analysis

Cells were solubilized in Laemmli's lysis buffer containing 2% sodium dodecyl sulfate (12). The suspension was resolved by electrophoresis, transferred to nitrocellulose sheets, and immunoblotted using a rabbit polyclonal antibody against glial fibrillary acidic protein (GFAP; G9269; Sigma) or mouse monoclonal antibodies against β-actin (A5441; Sigma), Stat3 (sc-8019; Santa Cruz Biotechnology, Santa Cruz, CA, USA), pStat3 (Tyr705-phosphorylated Stat3; sc-8059; Santa Cruz Biotechnology), SOCS3 (sc-9023; Santa Cruz Biotechnology), microtubule-associated protein 2 (MAP2; Sternberger Monoclonals, Lutherville, MD, USA), Tuj1 (MMS-435P; Covance Research, Berkeley, CA, USA), and Nestin (MAB353; Chemicon, Temecula, CA, USA) proteins. The second antibodies were alkaline phosphatase-conjugated anti-rabbit immunoglobulin G (IgG) for the rabbit polyclonal antibody or alkaline phosphatase-conjugated anti-mouse IgG for the mouse monoclonal antibodies. The density of immunoreac-

tive bands was measured using NIH image software (National Institutes of Health, Bethesda, MD, USA).

Luciferase promoter assay

The constructs of the Stat3 reporter plasmids have been described elsewhere (9). In brief, the Stat3F reporter plasmid contained 4 copies of the acute-phase response element (APRE) in front of the minimal junB promoter linked to the luciferase gene. The response element was the APRE of the rat α2-macroglobulin gene (5′-GCGCCTTCTGGGAAGATC-CTTACGGGAATTCAG-3′). The cultured neurospheres were washed once in PBS, triturated, and resuspended in the specified electroporation buffer to a final concentration of 1.0×10^7 cells/ml. Then, 10 μg Stat3 reporter plasmid and 4 μg pRL-TK (Promega) internal control plasmid DNA were mixed with 0.1 ml cell suspension, transferred to a 2.0-mm electroporation cuvette, and electroporated with an Amaxa Nucleofector apparatus (Amaxa, Cologne, Germany). Then transfected neurospheres were exposed to adenoviral vectors expressing SOC3, Stat3F, or Lz (MOI=10) for 1 h in differentiating medium or MCM. Some transfected neurospheres were treated with both mouse leukemia inhibitory factor (LIF; 30 ng/ml; Chemicon, Temecula, CA, USA) and human basic fibroblast growth factor (bFGF; 10 ng/ml; Genzyme Techne, Minneapolis, MN, USA) or both rat IL-6 (30 ng/ml; Peprotech, London, UK) and human sIL-6R (30 ng/ml, Peprotech) as a positive control. Two days after electroporation, the activity of firefly luciferase from the Stat3 promoter-luciferase plasmid and renilla luciferase from the pRL-TK plasmid in the cell extracts was evaluated using a dual-luciferase assay kit (Promega) with a luminometer (TD-20/20; Turner Designs, Sunnyvale, CA, USA). Relative firefly luciferase activity was calculated by normalizing the transfection efficiency according to the renilla luciferase activity.

Quantitative real-time PCR

Cells were washed with PBS, and total RNA was extracted using Isogen (Nippon Gene, Tokyo, Japan). Total RNA was digested with DNase, and then single-stranded cDNA was obtained using oligo dT primers and Moloney murine leukemia virus reverse transcriptase (Life Technologies, Rockville, MD, USA). For quantitative real-time PCR, TaqMan real-time PCR analysis was carried out. The oligonucleotide primers and TaqMan fluorogenic probe for each gene were purchased commercially (Applied Biosystems, Foster City, CA, USA; **Table 1**). Reactions were run on an ABI Prism 7700 sequence detection system (Applied Biosystems). The cycling conditions were 10 min polymerase activation at 95°C followed by 40 cycles at 95°C for 15 s and 60°C for 60 s. β-Actin was used as the internal control. Threshold cycle (Ct) values of the target genes were normalized to those of the internal control genes. The relative expression in each sample to that of the control sample was calculated according to the $2-\Delta\Delta CT$ method (13).

Immunocytochemistry

Cells were washed with PBS and fixed for 30 min with 4% paraformaldehyde in 0.1 M phosphate buffer (pH 7.4). After 3 washes with PBS, the samples were incubated with 10% normal goat serum dissolved in PBS. Either a primary mouse monoclonal antibody against MAP2 (Sternberger Monoclonals) or a rabbit polyclonal antibody against GFAP (Sigma) was incubated with the samples at 4°C overnight. The samples were washed 3 times with PBS, incubated with rhodamine-conjugated goat anti-mouse IgG (ICN, Irvine, CA, USA) or with fluorescein-5-isothiocyanate-conjugated goat anti-rabbit IgG (ICN) for 30 min at room temperature, washed 3 times with PBS and mounted in Vectashield (Vector Lab, Burlingame, CA, USA). The cells were counterstained with Hoechst 33342 (B2261; Sigma) to identify nuclei.

Enzyme-linked immunosorbent assay (ELISA) and NO assay

Microglial cells at a density of 4.0×10^5/ml were cultured for 24 h in neurosphere-differentiating medium. After their settlement was confirmed, cells were cultured with fresh neurosphere-differentiating media in the presence and absence of lipopolysaccharide (LPS; 1 μg/ml). One day later, the supernatants were collected and the assays were per-

TABLE 1. *Assay identifiers and gene names*

Assay ID	Gene name
Rn00667869_m1	β-actin
Rn00561420_m1	Interleukin 6
Rn00573491_g1	Leukemia inhibitory factor (LIF)
Rn00755092_m1	Ciliary neurotrophic factor (CNTF)
Rn00567503_m1	Cardiotrophin 1 (CT1)
Rn00567818_m1	Bone morphogenetic protein 2 (BMP2)
Rn00563202_m1	Bone morphogenetic protein 4 (BMP4)
Rn00570809_m1	Fibroblast growth factor 2 (FGF2)
Rn00563336_m1	Epidermal growth factor (EGF)
Rn01758634_g1	Notch 1
Rn00577522_m1	Notch 2
Rn00571731_m1	Notch 3
Rn00577566_m1	Hairy and enhancer of split 1 (Hes1)
Rn00821207_g1	Hairy and enhancer of split 5 (Hes5)
Rn00562985_s1	Inhibitor of DNA binding 1 (Id1)
Rn00564939_g1	Inhibitor of DNA binding 2 (Id2)
Rn00564927_m1	Inhibitor of DNA binding 3 (Id3)
Rn00574345_m1	Achaete-scute complex homolog-like 1 (Mash1)
Rn00824571_s1	Neurogenic differentiation 1 (NeuroD1)
Rn02132577_s1	Neurogenic differentiation 2 (NeuroD2)
Rn01751069_mH	SRY-box containing gene 9 (Sox9)

formed. The concentrations of IL-1β, IL-6, and tumor necrosis factor (TNF) -α in the supernatants were measured by ELISA. The nitrite levels were determined after mixing equal amounts of supernatant and Griess reagent [N-(1-naphthyl)-ethylenediamine (0.1%) and sulfanilamide (1%)] (Sigma). ELISA kits were purchased from BioSource USA (Camarillo, CA, USA) and used according to the manufacturer's protocol. Sodium nitrite (Sigma) was used as a standard solution.

Statistical analysis

All values are presented as means ± sd. The levels of nitrite and cytokines in the presence and absence of LPS were analyzed statistically by unpaired t test. All the other statistical significances were tested by one-way ANOVA followed by Bonferroni's multiple comparison test. A value of $P < 0.05$ was considered statistically significant.

RESULTS

Coculture with microglial cells promotes astrogliagenesis in NSCs

We first examined whether coculture of NSCs with microglial cells could modulate the differentiation of NSCs. To address this issue, microglial cells (0, 0.7×10^5, or 2.0×10^5/well) were directly added to NSC culture (5.0×10^5/well) in 24-well plates (mixed type). At 3 days after coculture, cells were homogenized in lysis buffer and immunoblotted with an antibody against GFAP (a specific marker of astrocytes) or MAP2 (a specific marker of neurons). Experiments were carried out 5 times independently. Densitometric analysis revealed that 3 days after coculture, the level of GFAP protein in NSCs with microglial cells (0.7×10^5 and 2.0×10^5/well) was significantly increased (~1.7- and 1.7-fold, respectively) compared with that in the control without microglial cells, whereas the level of MAP2 protein did not differ among the three groups (Fig. 1A–C).

To prevent physical interactions between NSCs and microglial cells, we performed another type of coculture in which the two cell populations were cultured in the same well, but were separated by a culture insert membrane that permitted medium exchange without physical contact between NSCs and microglial cells (insert type). Microglial cells (0, 0.7×10^5, or 2.0×10^5/well) were seeded into cell culture inserts that were placed on the top of a 24-well plate containing neurospheres. Three days after coculture, the level of GFAP protein in neurospheres with microglial cells was significantly increased (~2.0- and 2.2-fold) compared with that in the control without microglial cells, whereas the level of MAP2 protein did not differ among the three groups (Fig. 1D–F).

Because coculture study using culture inserts suggested that the effect of microglial cells on NSC differentiation was related to diffusible factors released by microglial cells in the medium, we next investigated the effects of MCM on the fate of NSCs. Medium in a 24-well plate containing neurospheres was changed to the conditioned medium from 24 h microglia cultures at a density of 0, 1.4 ×

10^5/ml, or 4.0×10^5/ml (conditioned type). Three days after culture with MCM, the level of GFAP protein in NSCs cultured with MCM (1.4×10^5/ml and 4.0×10^5/ml) was significantly increased (~1.8- and 1.7-fold) compared with that in the control without MCM, whereas the level of MAP2 protein did not differ among the three groups (Fig. 1G–I).

Taken together, these results showed that microglial cells promoted astrogliogenesis in NSCs and that this microglia-induced astrogliogenesis was not related to physical contact between the two cell populations but to some diffusible factors released by microglial cells. Hence, thereafter, we investigated the mechanisms of microglia-induced astrogliogenesis by using MCM (conditioned type).

AG490 inhibits microglia-induced astrogliogenesis in NSCs, whereas LY29002, PTPII, and Noggin do not

To clarify the mechanism of microglia-induced astrogliogenesis in NSCs, we applied reagents to inhibit the cell signaling for modulating the fate of NSCs. After NSCs were seeded into 24-well plates at a density of 5.0×10^5/well, they were incubated with MCM (conditioned medium from 24 h microglia cultures at a density of 1.4×10^5) in the presence and absence of these inhibitors. One or 3 days later, the cells were homogenized in lysis buffer and immunoblotted with antibodies against GFAP or MAP2. Experiments were carried out 5 times independently. Densitometric analysis revealed that a phosphoinositide 3-kinase (PI3K) inhibitor (10 μm/ml LY294002) did not inhibit microglia-induced astrogliogenesis (Fig. 2). Furthermore, a BMP-specific antagonist (20 ng/ml Noggin) and an SHP (Src homology 2 domain-containing tyrosine phosphatase) inhibitor (0.1 nm/ml PTP inhibitor II) did not inhibit this astrogliogenesis (Figs. 3 and 4). However, a Jak2 kinase inhibitor (1 μm/ml AG490) inhibited microglia-induced astrogliogenesis in NSCs (Fig. 5). Three days after incubation, the level of GFAP protein in NSCs with MCM was significantly increased (1.8-fold) compared with that in NSCs without MCM. With the addition of AG490, the level of GFAP protein was reduced to the control level (Fig. 5F). These results showed that the Jak/Stat signaling pathway played a crucial role in astrogliogenesis of NSCs mediated by microglial cells.

To confirm whether the increase of GFAP is really due to the increase of the number of astrocytes, we performed immunostaining for counting cell numbers. After NSCs were seeded into 24-well plates at a density of 2.0×10^5/well, they were incubated with neurosphere-differentiating medium or MCM in the presence or absence of AG490 (1 μm/ml). Three days later, expression of differentiation markers was evaluated by immunostaining with antibodies against GFAP and MAP2. Cells that were positive for MAP2 or GFAP were scored in 10 to 15 random nonoverlapping fields (400 μm²) in each experiment. The proportion of MAP2
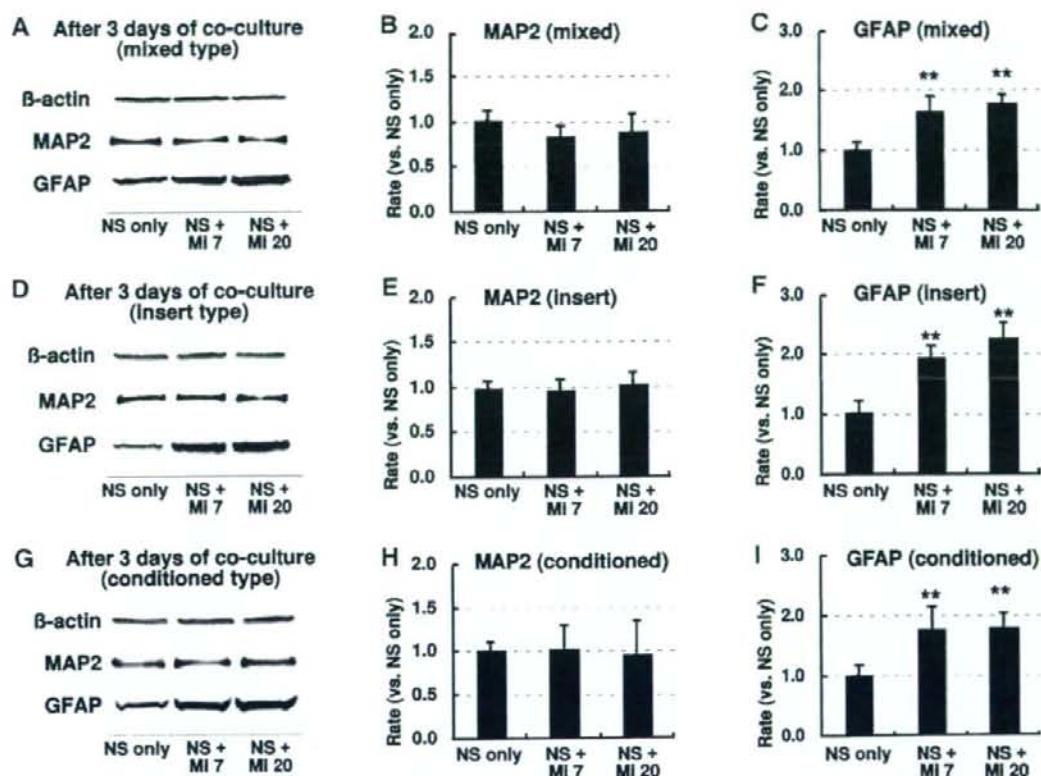
Figure 1. Effects of microglial (MI) cells on the fate of NSCs (NS) after 3 days of coculture. Microglial cells (0, 0.7×10^5, or 2.0×10^5/well) were directly added to NSC cultures (5.0×10^5/well) in 24-well plates (mixed type; *A–C*) or seeded into cell culture inserts that were placed on the top of a 24-well plate containing NSCs (insert type; *D–F*); or medium in a 24-well plate containing NSCs was changed to conditioned medium from 24 h microglia cultures at a density of 0, 1.4×10^5/ml, or 4.0×10^5/ml (conditioned type; *G–I*). At 3 days after coculture, cells were homogenized in lysis buffer and immunoblotted with an antibody against GFAP or MAP2. Experiments were carried out 5 times independently. Note that the protein level of GFAP was significantly increased in all three types of coculture. **$P < 0.01$ *vs.* NS only.
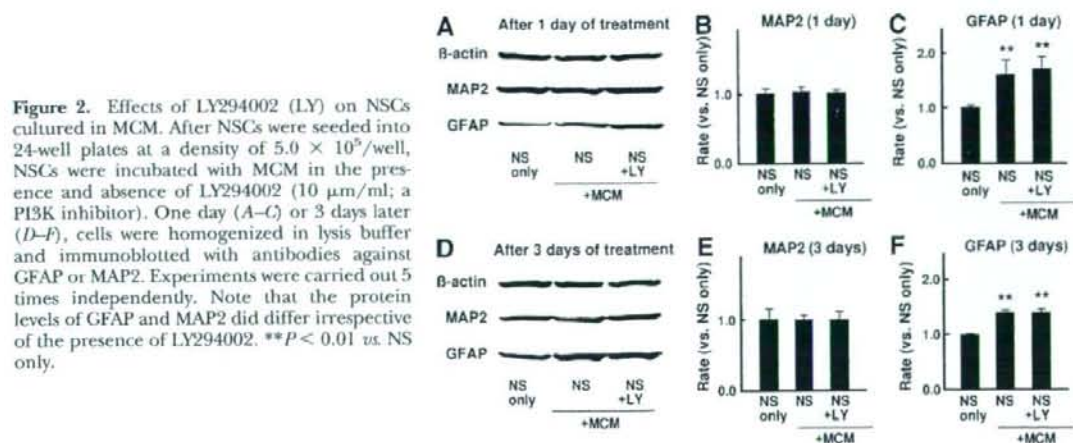
Figure 2. Effects of LY294002 (LY) on NSCs cultured in MCM. After NSCs were seeded into 24-well plates at a density of 5.0×10^5/well, NSCs were incubated with MCM in the presence and absence of LY294002 (10 μm/ml; a PI3K inhibitor). One day (*A–C*) or 3 days later (*D–F*), cells were homogenized in lysis buffer and immunoblotted with antibodies against GFAP or MAP2. Experiments were carried out 5 times independently. Note that the protein levels of GFAP and MAP2 did differ irrespective of the presence of LY294002. **$P < 0.01$ *vs.* NS only.
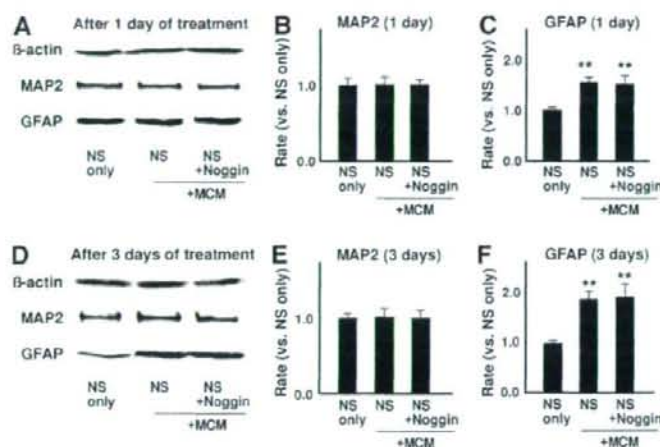
Figure 3. Effects of Noggin on NSCs cultured in MCM. After NSCs were seeded into 24-well plates at a density of 5.0×10^5/well, NSCs were incubated with MCM in the presence and absence of Noggin (20 ng/ml; a BMP-specific antagonist). One day (*A–C*) or 3 days later (*D–F*), cells were homogenized in lysis buffer and immunoblotted with antibodies against GFAP or MAP2. Experiments were carried out 5 times independently. Note that the protein levels of GFAP and MAP2 were not different irrespective of the presence of Noggin. **P < 0.01 *vs.* NS only.

and GFAP positive cells was expressed as a percentage of the MAP2 and GFAP positive cells to Hoechst 33342 positive cells, respectively. As shown in **Fig. 6**, MCM significantly increased the proportion of the GFAP-positive cells and this increase was inhibited by the treatment of AG490 [15.1±0.5% of total cells in neurosphere-differentiating medium, 34.2±0.6% in MCM, and 15.9±0.6% in MCM with AG490]. These data also suggested that MCM promoted astrogliogenesis of NSCs and that this MCM-induced astrogliogenesis was inhibited by AG490.

Stat3F and SOCS3 inhibit microglia-induced astrogliogenesis in NSCs

It is well known that Stat3 plays crucial roles in determining the fate of NSCs. Enhancement of Stat3 activity in NSCs leads to subsequent glial differentiation (14). Our inhibitor study showed that AG490, a Jak2 kinase inhibitor, suppressed microglia-induced astrogliogenesis, suggesting that the Jak/Stat signaling pathway, especially activation of Stat3 function, played a crucial

role in microglia-induced astrogliogenesis in NSCs. To confirm this assumption, we used two types of adenovirus vectors expressing Stat3F and SOCS3. Stat3F is a dominant-negative form of Stat3. In this mutant (Stat3F), the tyrosine residue at amino acid position 705 of murine Stat3 is mutated to phenylalanine. Stat3F binds to the gp130 receptor, which in turn leads to competitive inhibition of phosphorylation of endogenous Stat3 on activation of the gp130 receptor. When expressed at high levels, Stat3F has been shown to block activation of endogenous Stat3 in various types of cells including NSCs (10). SOCS3 has been shown to interact with gp130 and Jak, and this interaction results in relatively specific inhibition of gp130 signaling (15). Moreover, SOCS3 has been shown to block activation of endogenous Stat3 in NSCs (9).

By using these two types of adenovirus vectors, we examined whether microglia-induced astrogliogenesis was inhibited by blocking the activation of endogenous Stat3 in NSCs. After NSCs were seeded into 24-well plates at a density of 5.0×10^5/well, they were inoculated with an adenovirus vector expressing Stat3F,
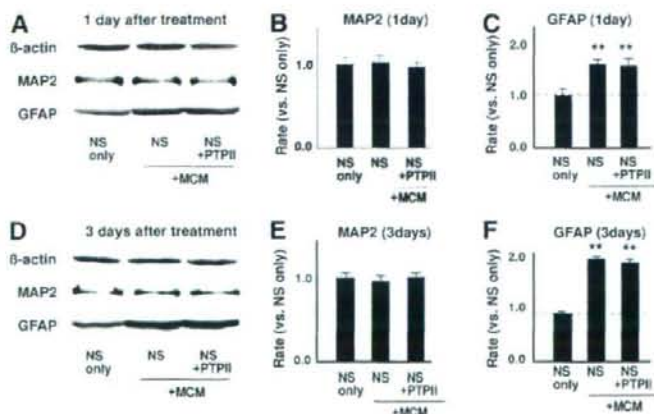

Figure 4. Effects of PTP inhibitor II on NSCs cultured in MCM. After NSCs were seeded into 24-well plates at a density of 5.0×10^5/well, NSCs were incubated with MCM in the presence and absence of a PTP inhibitor II (0.1 nm/ml PTPII; an SHP inhibitor). One day (*A–C*) or 3 days later (*D–F*), the cells were homogenized in lysis buffer and immunoblotted with antibodies against GFAP or MAP2. Experiments were carried out 5 times independently. Note that the protein levels of GFAP and MAP2 did not differ irrespective of the presence of PTP inhibitor II. **P < 0.01 *vs.* NS only.

Figure 5. Effects of AG490 (AG) on NSCs cultured in MCM. After NSCs were seeded into 24-well plates at a density of 5.0×10^5/well, NSCs were incubated with MCM (conditioned medium from 24 h microglia cultures at a density of 1.4×10^5/ml) in the presence and absence of AG490 (a Jak2 kinase inhibitor; 1 μm/ml). One day (A–C) or 3 days later (D–F), the cells were homogenized in lysis buffer and immunoblotted with antibodies against GFAP or MAP2. Experiments were carried out 5 times independently. Note that microglia-induced astrogliogenesis was significantly inhibited by AG490. *$P < 0.05$, **$P < 0.01$ vs. NS only.
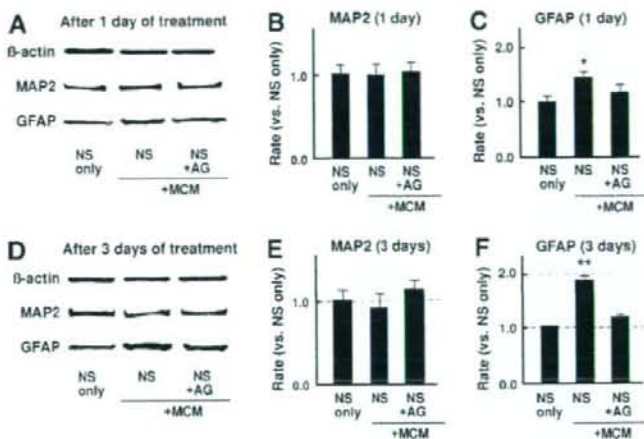
SOCS3, or LacZ (10 MOI each) and incubated with MCM (conditioned medium from 24 h microglia cultures at a density of 1.4×10^5/ml). Three days later, the cells were homogenized in lysis buffer and immunoblotted with an antibody against β-actin, SOCS3, Stat3, or pStat3 (Tyr705-phosphorylated Stat3).

Western blot analysis revealed that strong Stat3 and SOCS3 expression was evident in Ad.Stat3F- and Ad.SOCS3-infected cells but not in Ad.Lz-infected cells at 3 days after infection (**Fig. 7A**). Stat3 protein was expressed in both Ad.Lz- and Ad.SOCS3-infected cells. Moreover, pStat3 was weakly expressed in Ad.Lz-infected cells, but expression of pStat3 was not evident in Ad.Stat3F- and Ad.SOCS3-infected cells (Fig. 7A). These data suggest that overexpression of Stat3F and SOCS3 could suppress Stat3 cell signaling in NSCs.

We next examined whether overexpression of Stat3F and SOCS3 could modulate the differentiation of NSCs. At 3 days after infection, cells were homogenized in lysis buffer and immunoblotted with an antibody against GFAP, MAP2, or Nestin (a marker of NSCs). Experiments were carried out 5 times independently.

Densitometric analysis revealed that 3 days after infection, MCM significantly increased the level of GFAP protein in Ad.LacZ-infected cells (~3.4-fold), whereas the level of MAP2 protein did not differ among all groups (Fig. 7B, C). Furthermore, the level of GFAP protein in Ad.Stat3F- and Ad.SOCS3-infected cells cultured with MCM was significantly reduced (~1.7- and 5.2-fold, respectively), compared with that in Ad.Lz-infected cells cultured with MCM (Fig. 7B). These results suggested that microglia-induced astrogliogenesis was inhibited by blocking the activation of endogenous Stat3 in NSCs.

In addition, densitometric analysis revealed that 3 days after infection, MCM significantly increased the level of Nestin protein in Ad.LacZ-infected cells (~1.4-fold; Fig. 7D). Furthermore, compared with that in Ad.Lz-infected cells cultured without MCM, the level of Nestin protein in Ad.SOCS3-infected cells cultured

Figure 6. Effects of MCM on the fate of NSCs after 3 days of culture. After NSCs were seeded into 24-well plates at a density of 2.0×10^5/well, NSCs were incubated with neurosphere-differentiating medium (NM) or MCM in the presence or absence of AG490 (1 μm/ml). A–F) Three days later, expression of differentiation markers was evaluated by immunostaining with antibodies against GFAP (green; A, C, E) and MAP2 (red; B, D, F). To identify nuclei, cells were stained with Hoechst33342 (blue). Scale bar = 100 μm. Data were obtained from 5 independent measurements. Values represent means ± sd. G) GFAP-positive cells. H) MAP2-positive cells. **$P < 0.01$ vs. NM. Note that MCM significantly increased the proportion of the GFAP-positive cells and this increase was inhibited by the treatment of AG490.
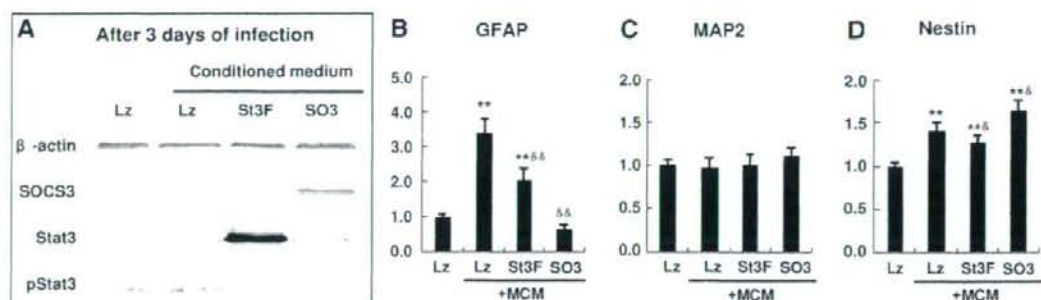
– 285 –
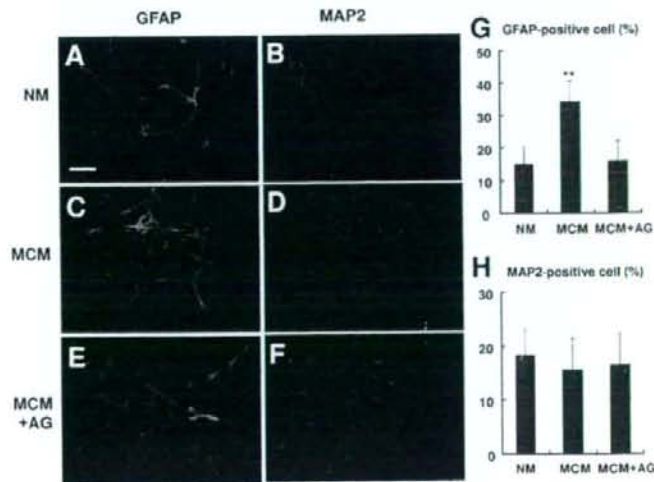
Figure 7. Effects of overexpression of Stat3F or SOCS3 on NSCs cultured in MCM. After NSCs were seeded into 24-well plates at a density of 5.0×10^5/well, NSCs were inoculated with adenovirus vector expressing Stat3F(St3F; a dominant negative form of Stat3), SOCS3(SO3), or LacZ(Lz) (10 MOI each) and incubated with MCM (conditioned medium from 24 h microglia cultures at a density of 1.4×10^5/ml). Three days later (A), the cells were homogenized in lysis buffer and immunoblotted with an antibody against β-actin, SOCS3, Stat3, pStat3 (Tyr705-phosphorylated Stat3), GFAP (B), MAP2 (C), or Nestin (D). Note that microglia-induced astrogliogenesis of NSCs was significantly inhibited by activation of endogenous Stat3 in NSCs. In addition, MCM significantly increased the protein level of Nestin in NSCs, and overexpression of SOCS3 induced an additional increase in Nestin protein. $**P < 0.01$ vs. Lz; $^\delta P < 0.05$, $^{\delta\delta}P < 0.01$ vs. Lz + MCM.

with MCM increased further (~1.6-fold; Fig. 7D). These results suggested that MCM promoted the maintenance of NSCs and SOCS3 accelerated this action.

Ramified microglial cells release neither NO nor inflammatory cytokines

To specify the properties of the microglial cells, we evaluated the amounts of NO and cytokines [interleukin (IL)-1β, IL-6, and TNF-α]. As shown in **Fig. 8B–E**, microglial cells in neurosphere-differentiating medium without LPS released little amounts of NO and inflammatory cytokines. Moreover, the shape of these microglial cells was a ramified form (Fig. 8A).

Real-time PCR for trophic factors in neurons, astrocytes, microglial cells, and NSCs

Because microglia-induced astrogliogenesis in NSCs appeared to occur through paracrine effects, we next investigated mRNA levels of several secreted trophic factors that are considered to modulate the fate of NSCs. We compared mRNA levels of several trophic factors among neurons, astrocytes, microglial cells, and NSCs by real-time PCR. Data were obtained from 4 independent experiments. Among the trophic factors examined, the expression of LIF and FGF2 mRNA in microglial cells was markedly upregulated (~78.0- and 28.4-fold increase, respectively), compared with those in NSCs (**Fig. 9**). Furthermore, microglial cells did not express IL-6, CT1, BMP4, and EGF mRNA in our experimental conditions. These results suggested that LIF and FGF2 were involved in the mechanism of microglia-induced astrogliogenesis in NSCs and that microglial cells were not activated in our experimental conditions.

Promoter assay with and without MCM

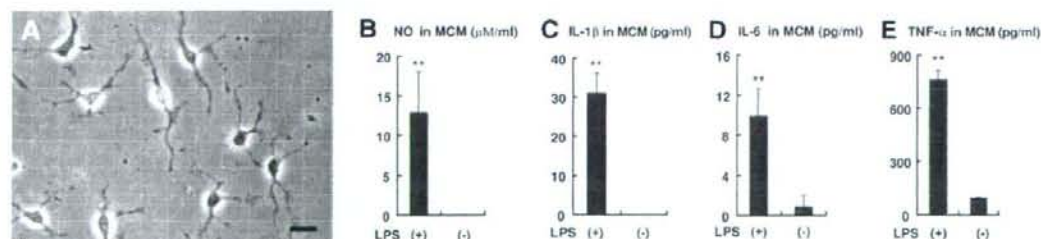To confirm whether MCM could actually activate Stat3 function in NSCs, minimal junB reporter constructs

Figure 8. Properties of microglial cells. Microglial cells at a density of 4.0×10^5/ml were cultured for 24 h in neurosphere-differentiating medium. After their settlement was confirmed (A), cells were cultured with fresh neurosphere-differentiating media in the presence and absence of LPS (1 μg/ml). One day later, the concentrations of NO (B) and cytokines [IL-1β (C), IL-6 (D), and TNF-α (E)] in the supernatants were measured by Griess reaction and ELISA, respectively. Note the microglial cells displaying a ramified morphology (A; scale bar=25 μm). Note that microglial cells in neurosphere-differentiating medium without LPS released little amounts of NO (B) and inflammatory cytokines [IL-1β (C), IL-6 (D), and TNF-α (E)]. $**P < 0.01$ vs. LPS(−).
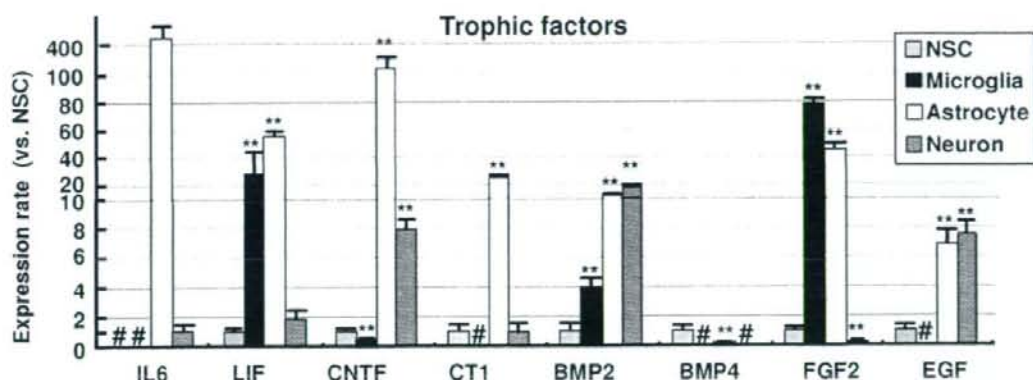
Figure 9. Expression of trophic factors in neurons, astrocytes, microglial cells, and NSCs. Cultured neurons, astrocytes, microglial cells, and NSCs were washed with PBS, and total RNA was extracted using Isogen (Nippon Gene). Total RNA was digested with DNase, and then single stranded cDNA was obtained using oligo dT primers and Moloney murine leukemia virus reverse transcriptase (Life Technologies). For quantitative real-time PCR, TaqMan real-time PCR analysis was carried out. The oligonucleotide primers and TaqMan fluorogenic probe for each gene were purchased commercially (Applied Biosystems; Table 1). The mRNA levels of several trophic factors were compared among neurons, astrocytes, microglial cells, and NSCs by real-time PCR. Data were obtained from 4 independent experiments. Note that expression of LIF and FGF2 in microglial cells was significantly upregulated, compared with that in NSCs. ∗∗$P < 0.01$ vs. NSC; #not detected.

with or without 4 copies of APRE were electroporated into the neurospheres. Then, the neurospheres were exposed to adenoviral vectors expressing SOCS3, Stat3F, or LacZ in the presence and absence of MCM. Two days later, dual luciferase assay was carried out. Experiments were carried out 5 times independently. After transfection of the Stat3 reporter plasmid (minimal junB promoter with 4 copies of APRE), relative luciferase activity in Ad.LacZ-, Ad.Stat3F-, Ad SOCS3- and Ad.LacZ + LIF + FGF2-treated NSCs cultured with MCM was significantly increased (~35.9-, 2.4-, 3.0-, and 2.0-fold, respectively) compared to that in Ad.LacZ-, Ad.Stat3F-, Ad.SOCS3-, and Ad.LacZ + LIF + FGF2-treated NSCs cultured without MCM, respectively (**Fig. 10A**). When NSCs were cultured without MCM, relative luciferase activity of Ad.Stat3F- and Ad.SOCS3-treated NSCs was significantly lower (~1.7- and 1.8-fold, respectively) than that of Ad.LacZ-treated NSCs, whereas relative luciferase activity of Ad.LacZ + LIF + FGF2-treated NSCs was significantly higher than that of Ad.LacZ-treated NSCs. When NSCs were cultured with MCM, the relative luciferase activity of Ad.Stat3F- and Ad.SOCS3-treated NSCs was significantly lower (~26.1- and 21.9-fold reduction, respectively) than that of Ad.LacZ-treated NSCs (Fig. 10A). However, after transfection of Stat3 control plasmid (minimal junB promoter without 4 copies of APRE), the relative luciferase activity did not differ among all groups (Fig. 10B). Taken together, these results proved that MCM, as well as treatment with LIF + FGF2, transactivated APRE and promoted Stat3 function. We also confirmed that overexpression of Stat3F and SOCS3 inhibited APRE transactivation via MCM and blocked Stat3 function.

Real-time PCR for Notch family members and inhibitory basic helix-loop-helix (bHLH) factors

Notch family members and inhibitory bHLH transcription factors play an important role in proliferation, cell lineage determination, and cell differentiation of NSCs (16). We therefore examined the effects of MCM on the mRNA levels of Notch family members (notch1, 2, and 3) as well as inhibitory bHLH transcription factors (hes1, hes5, id1, id2, and id3) in NSCs in the presence or absence of AG490. The mRNA levels in NSCs were evaluated using real-time PCR at 1 day after culture with MCM. Data were obtained from 4 independent experiments.

One day after culture with MCM, the mRNA levels of notch1–3, hes5, and id3 in NSCs were significantly increased (~3.4-, 1.8-, 2.5-, 1.4-, and 4.7-fold, respectively), compared with those in NSCs without MCM (**Fig. 11A**). Furthermore, after treatment with AG490, the mRNA levels of notch1, 2, and 3 in NSCs were significantly decreased (~1.6-, 1.5-, and 1.4-fold, respectively), whereas the mRNA level of hes5 was significantly increased further (~1.4-fold). Irrespective of treatment with AG490, the mRNA level of id3 in NSCs cultured with MCM was not changed.

Real-time PCR for proneural bHLH factors and Sox9 in NSCs

Proneural bHLH factors have been reported to block astrocyte differentiation (17), and in their absence, neural progenitors become astrocytes (18). On the contrary, Sox9 plays a crucial role in causing NSCs to switch from neurogenesis to gliogenesis (19). For these
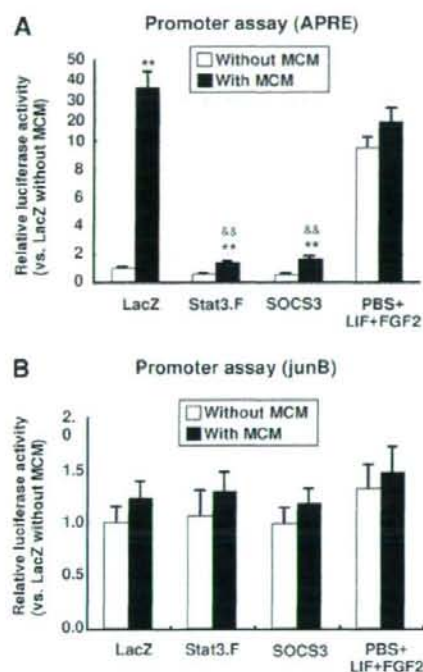
A

Promoter assay (APRE)

B

Promoter assay (junB)

Figure 10. Activation of Stat3 function in NSCs mediated by MCM. Minimal junB reporter constructs with (A) or without (B) 4 copies of APRE were electroporated into the neurospheres. Then NSCs cultured with MCM were exposed to adenoviral vectors expressing SOCS3, Stat3F, or LacZ. Two days later, dual luciferase assay was carried out. Experiments were carried out 5 times independently. Note that MCM, as well as treatment with LIF + FGF2, transactivated APRE and promoted Stat3 function. Furthermore, overexpression of Stat3F and SOCS3 inhibited APRE transactivation *via* MCM and blocked Stat3 function. $**P < 0.01$ *vs.* without MCM; $\&\&P < 0.01$ *vs.* LacZ with MCM.

reasons, we examined the effects of MCM on the mRNA levels of proneural bHLH factors (mash1, neuroD1, and neuroD2) and sox9 in NSCs.

One day after culture with MCM, mRNA levels of mash1, neuroD1, and neuroD2 were significantly decreased in NSCs ($\sim$1.9-, 1.4-, and 1.6-fold, respectively), whereas the mRNA level of Sox9 was significantly increased in NSCs ($\sim$1.3-fold; Fig. 11*B*). Treatment with AG490 significantly decreased mRNA levels of neuroD2 and sox9 ($\sim$1.6- and 2.0-fold, respectively) in NSCs cultured with MCM.

DISCUSSION

In the present study, we prepared three types of coculture of NSCs with microglial cells: mixed type, insert type, and conditioned type. In all types, microglial cells promoted astrogliogenesis, suggesting that their effects were not caused by physical contact between the two

cell populations but by some diffusible factors released by microglial cells. Our results differed from previous reports (20, 21) that microglial cells promoted neurogenesis in adult NSCs. One possible explanation is the difference in NSCs (*i.e.*, embryonic NSCs from the ganglionic eminences were used in our study whereas adult NSCs from the subventricular zone or the hippocampus were used in their studies). Another possible explanation is that the condition of microglial cells was different. It has been reported that both interferon-γ- and IL-4-activated microglial cells promoted neurogenesis of adult NSCs whereas LPS-activated microglial cells inhibited this neurogenesis (22). Moreover, macrophage colony-stimulating factor (M-CSF) -activated microglial cells promoted astrogliogenesis of NSCs (23). In our study, microglial cells were not activated by cytokines (such as interferon-γ and IL-4) or LPS. Consequently, IL-6 mRNA was not detected in microglial cells and little amounts of NO and inflammatory cytokines, such as IL-1β, IL-6, and TNF-α were detected in the conditioned medium. Furthermore, these microglia cells were displaying a ramified morphology. Thus, we demonstrated that ramified microglial cells promoted astrogliogenesis through their paracrine effects.

To investigate the cell signaling pathways of this microglia-induced astrogliogenesis of NSCs, we applied four types of reagents to inhibit the cell signaling for modulating the fate of NSCs. Consequently, a PI3K inhibitor (LY294002), a BMP-specific antagonist (Noggin), and an SHP inhibitor (PTP inhibitor II) did not inhibit this astrogliogenesis. Among them, only the Jak2 kinase inhibitor (AG490) inhibited microglia-induced astrogliogenesis in NSCs, suggesting a crucial role of the Jak-Stat signaling pathway in this mechanism. Subsequent studies, using adenovirus vectors, revealed that Stat3 (especially gp130 signaling) played a pivotal role in microglia-induced astrogliogenesis of NSCs. It is well known that Stat3 plays crucial roles in determining the fate of NSCs. Enhancement of Stat3 activity in NSCs leads to subsequent glial differentiation (14). LIF as well as ciliary neurotrophic factor (CNTF) and IL-6 can activate the Jak-Stat signaling pathway and promote astroglial differentiation (24). Phosphorylated Stat3 associates with the transcriptional coactivators CREB-binding protein (CBP/p300) to activate expression of astrocyte-specific genes (25). DNA methylation is also a critical determinant in the developmental stage-dependent regulation of astrocytogenesis (26). In this study, we showed that the level of LIF mRNA in microglial cells was significantly higher than that in NSCs, although the level of CNTF mRNA in microglial cells was significantly lower than that in NSCs, and neither IL-6 mRNA nor CT1 mRNA was detected in microglial cells. These data suggested that ramified microglial cells secreted LIF and promoted astrogliogenesis in NSCs.

We also showed that the level of FGF2 mRNA in microglial cells was significantly greater than that in NSCs. FGF2 was first purified as a heparin-binding polypeptide from bovine pituitary and was subsequently
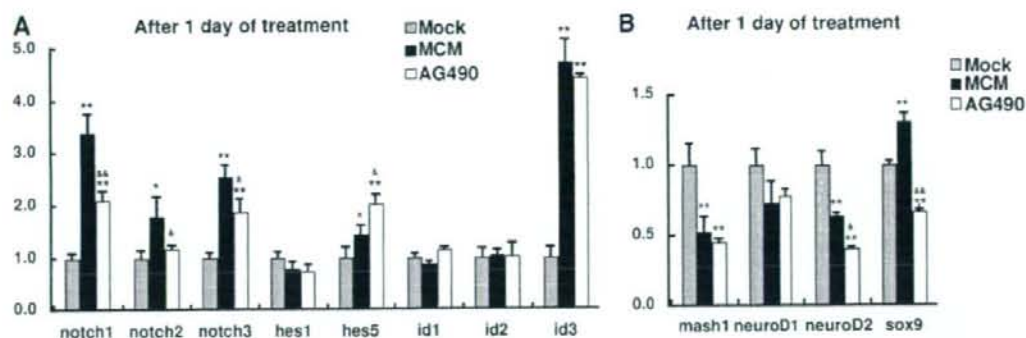
Figure 11. mRNA expression profiles of notch family, bHLH factors, or sox9 after 1 day of treatment with MCM in the presence or absence of AG490. After NSCs were seeded into 24-well plates at a density of 5.0×10^5/well, NSCs were incubated with MCM in the presence and absence of AG490 (a Jak2 kinase inhibitor; 1 μm/ml). As a control, NSCs were incubated only with neurosphere-differentiating medium (mock). One day later, total RNA was extracted using Isogen (Nippon Gene). Total RNA was digested with DNase, and then single-stranded cDNA was obtained using oligo dT primers and Moloney murine leukemia virus reverse transcriptase (Life Technologies). For quantitative real-time PCR, TaqMan real-time PCR analysis was carried out. The oligonucleotide primers and TaqMan fluorogenic probe for each gene were purchased commercially (Applied Biosystems; Table 1). Data were obtained from 4 independent experiments. Note that expression of notch1–3 (A) and sox9 (B) was significantly upregulated after treatment with MCM, and this up-regulation was significantly inhibited by AG490. $*P < 0.05$, $**P < 0.01$ vs. Mock; $\&P < 0.05$, $\&\&P < 0.01$ vs. MCM.

characterized as a basic protein of 18 kDa (27). FGF-2 is a strong promoter of fibroblast proliferation. However, most of the interest in FGF-2 stems from its pleiotropic effects. FGF-2 is one of the most potent angiogenic factors, possesses neuroprotective properties, and is implicated in vascular remodeling and tumor metastasis (28). It has been shown that the *in vitro* expansion and differentiation of NSCs can be regulated by adding FGF2 to the culture medium (29). Moreover, it has been reported that FGF2 is expressed in the dorsolateral cortical neuroepithelium of the forebrain and FGF2 is one of the most potent mitogens and survival factors for cultured NSCs (30). As well as FGF-2, LIF is also known to be required for long-term maintenance of NSCs (31). In our study, we demonstrated that the level of Nestin protein in NSCs was significantly increased by treatment with MCM, suggesting that ramified microglia-derived LIF and FGF2 promoted the maintenance of NSCs.

To clarify the molecular mechanisms underlying microglia-induced astrogliogenesis, we investigated the expression of Notch family members bHLH transcription factors, and sox9 genes. Notch family members and bHLH transcription factors play important roles in proliferation, cell lineage determination and cell differentiation of NSCs (16). Several investigators have shown interactions between the Stat3 and Notch pathways. It has been reported that activation of glycoprotein 130 (gp130; a common receptor component of IL-6 family cytokines) stimulates the Notch1 pathway, increasing the expression of hairy-enhancer-of-split 1 (Hes1; ref. 32). It has also been demonstrated that Stat3 is an essential effector of Notch-Hes signaling (33). Furthermore, it has been reported that the notch ligand delta-like 1 (DLL1) is a key target of Stat3 in both inhibition of neurogenesis and maintenance of

NSCs, which may underlie the noncell-autonomous action of Stat3 in inhibiting neuronal differentiation (34). In this study, we showed significant up-regulation of notch 1, 2, and 3 mRNA at 1 day after treatment with MCM, and this up-regulation was significantly inhibited by the Jak2 inhibitor, AG490, whereas hes1 and hes5 mRNA were not. We cannot explain why the temporal profiles of hes1 and hes5 mRNA (downstream genes of notch signaling) were not the same as those of notch1–3 mRNA. However, neurospheres could be generated from embryos mutant for hes1 and hes5. Hes1 and hes5 double-mutant neurospheres still demonstrated self-renewal (35). It has also been reported that neither hes1 nor hes5 mediates gp-130-enhanced notch signaling that regulates NSC maintenance (32). These results support the contention that besides the Notch-Hes pathway other signaling pathways can mediate notch signaling in the maintenance and differentiation of NSCs.

In addition, it is well known that Sox9 plays a crucial role in chondrocyte development and male sex determination (36). Recently, it has been demonstrated that Sox9 is essential for proper development of both oligodendrocytes and astrocytes and suggested that Sox9 is a component of the mechanism that causes NSCs to switch from neurogenesis to gliogenesis (19). Sox9 has also been implicated in maintaining cells in a stem cell-like state and preventing their exit from the cell cycle and the induction of neurogenesis (37). Furthermore, notch signaling is required for the maintenance of Sox9 expression during the gliogenic phase of spinal cord development (38). Consistent with these previous reports, our data showed that MCM-induced up-regulation of sox9 and notch1–3 promotes astrogliogenesis and maintenance of NSCs.

In conclusion, we have demonstrated that ramified

microglial cells promote astrogliogenesis and maintenance of NSCs through their paracrine effects and that their effects are caused by activation of Stat3 function. This finding of active roles of microglial cells is unexpected and raises the possibility that neuronal production in the brain is regulated, at least in part, by the regional properties of microglial cells. 🎦

REFERENCES

1. Alvarez-Buylla, A., and Lim, D. A. (2004) For the long run: maintaining germinal niches in the adult brain. *Neuron* 41, 683–686

2. Song, H., Stevens, C. F., and Gage, F. H. (2002) Astroglia induce neurogenesis from adult neural stem cells. *Nature* 417, 39–44

3. Aarum, J., Sandberg, K., Haeberlein, S. L., and Persson, M. A. (2003) Migration and differentiation of neural precursor cells can be directed by microglia. *Proc. Natl. Acad. Sci. U. S. A.* 100, 15983–15988

4. Ziv, Y., Ron, N., Butovsky, O., Landa, G., Sudai, E., Greenberg, N., Cohen, H., Kipnis, J., and Schwartz, M. (2006) Immune cells contribute to the maintenance of neurogenesis and spatial learning abilities in adulthood. *Nat. Neurosci.* 9, 268–275

5. Aloisi, F. (2001) Immune function of microglia. *Glia* 36, 165–179

6. Streit, W. J. (2002) Microglia as neuroprotective, immunocompetent cells of the CNS. *Glia* 40, 133–139

7. Polazzi, E., and Contestabile, A. (2002) Reciprocal interactions between microglia and neurons: from survival to neuropathology. *Rev. Neurosci.* 13, 221–242

8. Suzumura, A., Mezitis, S. G., Gonatas, N. K., and Silberberg, D. H. (1987) MHC antigen expression on bulk isolated macrophage-microglia from newborn mouse brain: induction of Ia antigen expression by gamma-interferon. *J. Neuroimmunol.* 15, 263–278

9. Cao, F., Hata, R., Zhu, P., Ma, Y. J., Tanaka, J., Hanakawa, Y., Hashimoto, K., Niinobe, M., Yoshikawa, K., and Sakanaka, M. (2006) Overexpression of SOCS3 inhibits astrogliogenesis and promotes maintenance of neural stem cells. *J. Neurochem.* 98, 459–470

10. Gu, F., Hata, R., Ma, Y. J., Tanaka, J., Mitsuda, N., Kumon, Y., Hanakawa, Y., Hashimoto, K., Nakajima, K., and Sakanaka, M. (2005) Suppression of Stat3 promotes neurogenesis in cultured neural stem cells. *J. Neurosci. Res.* 81, 163–171

11. Kanegae, Y., Makimura, M., and Saito, I. (1994) A simple and efficient method for purification of infectious recombinant adenovirus. *Jpn. J. Med. Sci. Biol.* 47, 157–166

12. Laemmli, U. K. (1970) Cleavage of structural proteins during the assembly of the head of bacteriophage T4. *Nature* 227, 680–685

13. Livak, K. J., and Schmittgen, T. D. (2001) Analysis of relative gene expression data using real-time quantitative PCR and the 2[-Delta Delta C(T)] method. *Methods* 25, 402–408

14. Rajan, P., and McKay, R. D. (1998) Multiple routes to astrocytic differentiation in the CNS. *J. Neurosci.* 18, 3620–3629

15. Schmitz, J., Weissenbach, M., Haan, S., Heinrich, P. C., and Schaper, F. (2000) SOCS3 exerts its inhibitory function on interleukin-6 signal transduction through the SHP2 recruitment site of gp130. *J. Biol. Chem.* 275, 12848–12856

16. Lasky, J. L., and Wu, H. (2005) Notch signaling, brain development, and human disease. *Pediatr. Res.* 57, 104R–109R

17. Sun, Y., Nadal-Vicens, M., Misono, S., Lin, M. Z., Zubiaga, A., Hua, X., Fan, G., and Greenberg, M. E. (2001) Neurogenin promotes neurogenesis and inhibits glial differentiation by independent mechanisms. *Cell* 104, 365–376

18. Nieto, M., Schuurmans, C., Britz, O., and Guillemot, F. (2001) Neural bHLH genes control the neuronal versus glial fate decision in cortical progenitors. *Neuron* 29, 401–413

19. Stolt, C. C., Lommes, P., Sock, E., Chaboissier, M. C., Schedl, A., and Wegner, M. (2003) The Sox9 transcription factor determines glial fate choice in the developing spinal cord. *Genes Dev.* 17, 1677–1689

20. Battista, D., Ferrari, C. C., Gage, F. H., and Pitossi, F. J. (2006) Neurogenic niche modulation by activated microglia: transforming growth factor beta increases neurogenesis in the adult dentate gyrus. *Eur. J. Neurosci.* 23, 83–93

21. Walton, N. M., Sutter, B. M., Laywell, E. D., Levkoff, L. H., Kearns, S. M., Marshall, G. P., 2nd, Scheffler, B., and Steindler, D. A. (2006) Microglia instruct subventricular zone neurogenesis. *Glia* 54, 815–825

22. Butovsky, O., Ziv, Y., Schwartz, A., Landa, G., Talpalar, A. E., Pluchino, S., Martino, G., and Schwartz, M. (2006) Microglia activated by IL-4 or IFN-gamma differentially induce neurogenesis and oligodendrogenesis from adult stem/progenitor cells. *Mol. Cell. Neurosci.* 31, 149–160

23. Nakanishi, M., Niidome, T., Matsuda, S., Akaike, A., Kihara, T., and Sugimoto, H. (2007) Microglia-derived interleukin-6 and leukaemia inhibitory factor promote astrocytic differentiation of neural stem/progenitor cells. *Eur. J. Neurosci.* 25, 649–658

24. Bonni, A., Sun, Y., Nadal-Vicens, M., Bhatt, A., Frank, D. A., Rozovsky, I., Stahl, N., Yancopoulos, G. D., and Greenberg, M. E. (1997) Regulation of gliogenesis in the central nervous system by the JAK-STAT signaling pathway. *Science* 278, 477–483

25. Nakashima, K., Yanagisawa, M., Arakawa, H., Kimura, N., Hisatsune, T., Kawabata, M., Miyazono, K., and Taga, T. (1999) Synergistic signaling in fetal brain by STAT3-Smad1 complex bridged by p300. *Science* 284, 479–482

26. Taga, T., and Fukuda, S. (2005) Role of IL-6 in the neural stem cell differentiation. *Clin. Rev. Allergy Immunol.* 28, 249–256

27. Abraham, J. A., Mergia, A., Whang, J. L., Tumolo, A., Friedman, J., Hjerrild, K. A., Gospodarowicz, D., and Fiddes, J. C. (1986) Nucleotide sequence of a bovine clone encoding the angiogenic protein, basic fibroblast growth factor. *Science* 233, 545–548

28. Yu, P. J., Ferrari, G., Galloway, A. C., Mignatti, P., and Pintucci, G. (2007) Basic fibroblast growth factor (FGF-2): the high molecular weight forms come of age. *J. Cell. Biochem.* 100, 1100–1108

29. Gage, F. H., Coates, P. W., Palmer, T. D., Kuhn, H. G., Fisher, L. J., Suhonen, J. O., Peterson, D. A., Suhr, S. T., and Ray, J. (1995) Survival and differentiation of adult neuronal progenitor cells transplanted to the adult brain. *Proc. Natl. Acad. Sci. U. S. A.* 92, 11879–11883

30. Dono, R. (2003) Fibroblast growth factors as regulators of central nervous system development and function. *Am. J. Physiol. Regul. Integr. Comp. Physiol.* 284, R867–R881

31. Shimazaki, T., Shingo, T., and Weiss, S. (2001) The ciliary neurotrophic factor/leukemia inhibitory factor/gp130 receptor complex operates in the maintenance of mammalian forebrain neural stem cells. *J. Neurosci.* 21, 7642–7653

32. Chojnacki, A., Shimazaki, T., Gregg, C., Weinmaster, G., and Weiss, S. (2003) Glycoprotein 130 signaling regulates Notch1 expression and activation in the self-renewal of mammalian forebrain neural stem cells. *J. Neurosci.* 23, 1730–1741

33. Kamakura, S., Oishi, K., Yoshimatsu, T., Nakafuku, M., Masuyama, N., and Gotoh, Y. (2004) Hes binding to STAT3 mediates crosstalk between Notch and JAK-STAT signalling. *Nat. Cell Biol.* 6, 547–554

34. Yoshimatsu, T., Kawaguchi, D., Oishi, K., Takeda, K., Akira, S., Masuyama, N., and Gotoh, Y. (2006) Non-cell-autonomous action of STAT3 in maintenance of neural precursor cells in the mouse neocortex. *Development* 133, 2553–2563

35. Ohtsuka, T., Sakamoto, M., Guillemot, F., and Kageyama, R. (2001) Roles of the basic helix-loop-helix genes Hes1 and Hes5 in expansion of neural stem cells of the developing brain. *J. Biol. Chem.* 276, 30467–30474

36. Bi, W., Deng, J. M., Zhang, Z., Behringer, R. R., and de Crombrugghe, B. (1999) Sox9 is required for cartilage formation. *Nat. Genet.* 22, 85–89

37. Seymour, P. A., Freude, K. K., Tran, M. N., Mayes, E. E., Jensen, J., Kist, R., Scherer, G., and Sander, M. (2007) SOX9 is required for maintenance of the pancreatic progenitor cell pool. *Proc. Natl. Acad. Sci. U. S. A.* 104, 1865–1870

38. Taylor, M. K., Yeager, K., and Morrison, S. J. (2007) Physiological Notch signaling promotes gliogenesis in the developing peripheral and central nervous systems. *Development* 134, 2435–2447

Correspondence

A marked increase in serum soluble Fas ligand in drug-induced hypersensitivity syndrome

Sɪʀ, The mechanism of epidermal necrosis in Stevens–Johnson syndrome (SJS) and toxic epidermal necrolysis (TEN) has long been controversial. The classical hypothesis is that of the involvement of cytotoxic T cells.[1,2] However, few of these cells infiltrate the SJS/TEN lesional skin,[3,4] and they induce apoptosis mainly in attached target cells through perforin/granzyme.[5] Therefore, the involvement of cytotoxic T cells alone cannot fully explain the extensive apoptosis of the SJS/TEN epidermis.

Recently, the possible involvement of soluble Fas ligand (sFasL) in SJS/TEN has been discussed.[6,7] Human keratinocytes express Fas, one of the death receptors, and the Fas–FasL interaction induces apoptosis in keratinocytes.[8] Abe et al. reported a significant elevation of the sFasL levels in serum from patients with TEN and SJS, but not from those with maculopapular eruption (MPE) or normal controls.[7] Furthermore, they demonstrated that the serum of patients with TEN induced keratinocyte apoptosis in vitro, and the effect was blocked by the addition of anti-FasL antibodies.

However, Stur et al. questioned the involvement of the Fas–sFasL interaction in SJS/TEN. They detected high sFasL levels in some patients with MPE, as well as SJS, while the sFasL levels of patients with TEN were rather low.[9] This led us to ask whether the increased serum sFasL level is specific for SJS/TEN. To address this question, we examined the sFasL levels in serial serum samples from patients with drug-induced hypersensitivity syndrome (DIHS)/drug rash with eosinophilia and systemic symptoms, another severe adverse drug reaction, and compared them with sFasL levels in patients with MPE and SJS/TEN.

Serial serum samples were obtained from 12 patients who were diagnosed with DIHS, SJS/TEN or MPE (four patients each). All these patients were treated at our inpatient clinic between 2000 and 2006. They were admitted to our hospital in the early stage of an adverse drug reaction, or developed the adverse drug reaction during their hospitalization for pre-existing diseases. The patient characteristics are listed in Table 1. The diagnosis of DIHS was based on the reported diagnostic criteria for DIHS.[10] Human herpesvirus 6 (HHV-6)

Table 1 Characteristics of the patients with drug-induced hypersensitivity syndrome (DIHS), Stevens–Johnson syndrome/toxic epidermal necrolysis (SJS/TEN) and maculopapular eruption (MPE)

Patient	Age (years)/sex	Diagnosis	Causative drug	Clinical signs and symptoms	Initial treatment
1	67/M	DIHS	Allopurinol	Fever, liver dysfunction (ALT 141 IU mL^{-1}), lymphadenopathy, HHV-6 reactivation	PSL 30 mg
2	69/M	DIHS	Carbamazepine	Fever, liver dysfunction (ALT 668 IU mL^{-1}), HHV-6 reactivation	No systemic steroid
3	33/F	DIHS	Carbamazepine	Fever, liver dysfunction (ALT 1202 IU mL^{-1}), lymphadenopathy, HHV-6 reactivation	PSL 60 mg
4	30/M	DIHS	Phenobarbital	Fever, liver dysfunction (ALT 308 IU mL^{-1}), lymphadenopathy, HHV-6 reactivation	mPSL pulse[a]
5	67/M	TEN[c]	Cyclophosphamide	10% epidermal detachment, mucosal involvement	mPSL pulse[a] + γ-glb[b]
6	71/M	SJS	Allopurinol	5% epidermal detachment, mucosal involvement	mPSL pulse[a]
7	43/M	SJS	Loxoprofen sodium, sodium valproate	3% epidermal detachment, mucosal involvement, liver dysfunction (ALT 507 IU mL^{-1})	mPSL pulse[a] + γ-glb[b]
8	72/M	SJS	Allopurinol	3% epidermal detachment, mucosal involvement	mPSL pulse[a]
9	68/F	MPE	Phenytoin	No systemic symptoms	No systemic steroid
10	69/M	MPE	Phenytoin	No systemic symptoms	No systemic steroid
11	76/M	MPE	Allopurinol	Fever	No systemic steroid
12	43/F	MPE	Carbamazepine	Fever, liver dysfunction (ALT 615 IU mL^{-1})	PSL 30 mg

ALT, alanine aminotransferase; HHV-6, human herpesvirus 6; PSL, prednisolone; mPSL, methylprednisolone; γ-glb, gamma-globulin. [a]mPSL pulse: 1 g daily for 3 days. [b]γ-glb: 0·1 g kg^{-1} daily for 3 days. [c]Patient 5 had widespread erythema on the whole body, and a markedly positive Nikolsky sign. In addition, typical epidermal necrosis was observed when skin biopsy was performed in an erythematous lesion without bullous or erosive change.

1

reactivation was confirmed by a significant increase in anti-HHV-6 IgG titre or the appearance of HHV-6 DNA in patients' blood. Patients with SJS and TEN showed mucosal involvement and epidermal detachment to various degrees. Epidermal necrosis was confirmed by skin biopsy in all of the patients with SJS and TEN. The serum samples were stored at -20 °C until use. The sFasL in the serum samples was measured using sandwich enzyme-linked immunosorbent assay (ELISA) kits purchased from R&D Systems (Minneapolis, MN, U.S.A.). The detection limit was 16 pg mL^{-1}. The mean ± SD level of serum sFasL was 68 ± 39 pg mL^{-1} in 13 normal controls.

Increased sFasL was revealed in the early phase of DIHS, as well as in SJS/TEN and MPE (Fig. 1). Note that ours is the first report to examine sFasL in serial samples from patients with DIHS and MPE. Interestingly, the greatest mean ± SD level of sFasL was higher in patients with DIHS (268 ± 90 pg mL^{-1})

than in those with SJS/TEN (181 ± 41 pg mL^{-1}) or MPE (159 ± 58 pg mL^{-1}). In addition, patients with severe DIHS had higher sFasL levels than those with mild DIHS. The disease was clinically more severe in DIHS patients 3 and 4 than in DIHS patients 1 and 2. Patients 3 and 4 required high-dose systemic corticosteroid therapy due to high fever, severe liver dysfunction and erythroderma. Although patient 2 had a high alanine aminotransferase level, the other signs and symptoms were mild.

In the patients with SJS/TEN, a marked rise in sFasL levels occurred within approximately 4 days after the onset of the skin rash, except for patient 7, in whom the peak of sFasL was observed at the 7th day. The causative drugs were stopped within 2 days after the onset of the rash in patients 5, 6 and 8, but on the fourth day in patient 7, which might have delayed the appearance of the highest peak of sFasL.
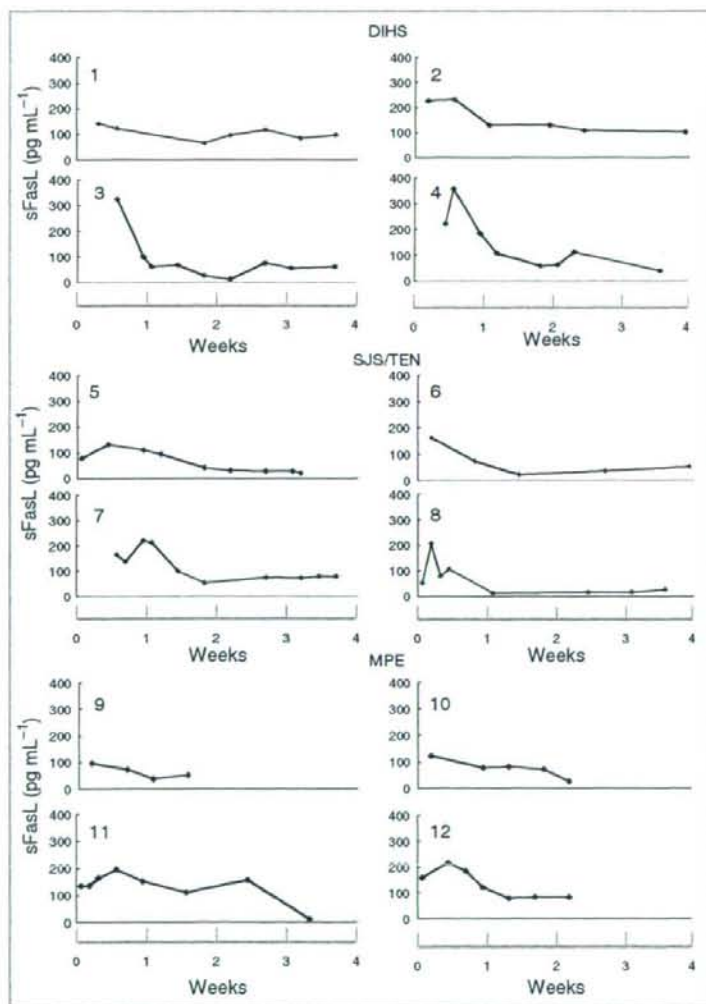

Fig 1. Soluble Fas ligand (sFasL) was measured in serial serum samples from patients with drug-induced hypersensitivity syndrome (DIHS), Stevens–Johnson syndrome/toxic epidermal necrolysis (SJS/TEN) and maculopapular eruption (MPE). The x-axis refers to time after onset of the disease. The figures show serial sFasL levels over a 4-week period.

In patients with MPE, similar to DIHS, the patients with milder disease, with no systemic symptoms (patients 9 and 10), had lower sFasL levels compared with the patients with more severe disease, with systemic symptoms (patients 11 and 12). Therefore, it seems likely that the sFasL levels correlate with the severity of the adverse drug reaction, regardless of whether the patient has DIHS, SJS/TEN or MPE. Abe et al. showed that the peripheral blood mononuclear cells (PBMC) of patients with TEN expressed FasL mRNA on stimulation with the causative drug.[7] The expression of FasL by PBMC stimulated by the causative drug may be a common feature in all types of drug eruption, including DIHS, MPE and SJS/TEN. In other words, strong allergic sensitization may cause the release of a large amount of sFasL from PBMC.

In the report of Abe et al.,[7] sFasL was undetectable in serum from patients with MPE. However, we detected an increase in sFasL levels in patients with MPE. This discrepancy might have been caused by a difference in ELISA kits. Our ELISA kit had high sensitivity at low concentrations.

In conclusion, our data suggest that elevated sFasL levels may be seen not only in SJS/TEN, but also in DIHS and MPE. There appears to be a correlation with disease severity, although data for a larger cohort of patients are needed to confirm this.

Acknowledgments

Department of Dermatology,   M. TOHYAMA
Ehime University Graduate School of Medicine,   Y. SHIRAKATA
Toon-city, Ehime 791-0295, Japan   K. SAYAMA
E-mail: tohm@m.ehime-u.ac.jp   K. HASHIMOTO

References

1 Friedmann PS, Strickland I, Pirmohamed M et al. Investigation of mechanisms in toxic epidermal necrolysis induced by carbamazepine. Arch Dermatol 1994; 130:598–604.

2 Le Cleach L, Delaire S, Boumsell L et al. Blister fluid T lymphocytes during toxic epidermal necrolysis are functional cytotoxic cells which express human natural killer (NK) inhibitory receptors. Clin Exp Immunol 2000; 119:225–30.

3 Miyauchi H, Hosokawa H, Akaeda T et al. T-cell subsets in drug-induced toxic epidermal necrolysis. Arch Dermatol 1991; 127: 851–5.

4 Murata J, Abe R. Soluble Fas ligand: is it a critical mediator of toxic epidermal necrolysis and Stevens-Johnson syndrome? J Invest Dermatol 2007; 127:744–5.

5 Catalfamo M, Henkart PA. Perforin and the granule exocytosis cytotoxicity pathway. Curr Opin Immunol 2003; 15:522–7.

6 Viard I, Wehrli P, Bullani R et al. Inhibition of toxic epidermal necrolysis by blockade of CD95 with human intravenous immunoglobulin. Science 1998; 282:490–3.

7 Abe R, Shimizu T, Shibaki A et al. Toxic epidermal necrolysis and Stevens-Johnson syndrome are induced by soluble Fas ligand. Am J Pathol 2003; 162:1515–20.

8 Viard-Leveugle I, Bullani RR, Meda P et al. Intercellular localization of keratinocyte Fas ligand explains lack of cytolytic activity under physiological conditions. J Biol Chem 2003; 278:16183–8.

9 Stur K, Karlhofer FM, Stingl G. Soluble FAS ligand: a discriminating feature between drug-induced skin eruptions and viral exanthemas. J Invest Dermatol 2007; 127:802–7.

10 Shiohara T, Iijima M, Ikezawa Z, Hashimoto K. The diagnosis of a DRESS syndrome has been sufficiently established on the basis of typical clinical features and viral reactivations. Br J Dermatol 2007; 156:1083–4.